

Vladimir Ivannikov
Helmholtz-Zentrum Hereon,
Institute of Metallic Biomaterials,
Department of Powder-based Materials
Development,
Max-Planck-Straße 1,
21502 Geesthacht, Germany
e-mail: vladimir.ivannikov@hereon.de

Mikhail Leontiev
Moscow Aviation Institute,
Department of Engine Design and Engineering,
Volokolamskoe Shosse 4,
125993 Moscow, Russia
e-mail: lemkn@alfatran.com

Sergey Degtyarev
Alfa-Transit Co. Ltd.,
Leningradskaya Street 1,
141400 Khimki, Russia
e-mail: degs@alfatran.com

Valeriy Popov
Department of Applied Mechanics,
Bauman Moscow State Technical University,
2-nd Baumanskaya Street 5-1,
105005 Moscow, Russia
e-mail: vpopov@bmstu.ru

Analysis of Radial Roller Bearing Rating Life in Complex Loading Conditions

An approach for accurate life analysis of radial roller bearings in complex loading conditions is presented. It employs ISO 16281 and accounts not only for external radial loads applied to the inner ring but also for (i) internal bearing clearance, (ii) flexibility of the bearing rings, (iii) rings out-of-roundness, (iv) inertia effects, (v) rolling elements profile, and (vi) rings misalignment. In the last decades, these factors have been becoming more and more important for modern high-performance jet engines, whose shafts are commonly hollow and the housing and the rings thicknesses may be of comparable magnitudes. To obtain the distribution of internal contact forces, an advanced static model of a bearing with deformable, potentially misaligned, rings is developed. The bending deformations of the rings are reproduced superimposing deformed shapes from each of the arising internal contact force applied individually. Bearing rollers are allowed to have non-cylindrical profile, and its geometry is approximated by means of slices each having constant diameter. A robust numerical scheme for solving the resultant set of equations with the aid of the barrier functions method is constructed. To increase even further the accuracy of rating life analysis, distributions of the contact stresses between the roller and the ring surfaces, obtained by solving numerically the problem of non-Hertzian interaction, are added to computations. A numerical benchmark test is presented to demonstrate the applicability of the developed approach. It shows how the aforementioned factors influence the bearing contact forces and its rating life. [DOI: 10.1115/1.4051201]

Keywords: bearings, rolling element bearings, bearing life

1 Introduction

When a rolling bearing is being designed for a particular rotating machine, it is essential to provide reliable assessments of its rating life. Most of the currently widely approaches aimed to tackle this issue rely on the life theory of Lundberg and Pamlgren [1,2]. They managed to construct an elegant and beautiful formulation which resulted in a classical formula for computing the basic rating life of ball and roller bearings:

$$L_{10r} = \left(\frac{C_r}{F_{eq}} \right)^d \quad (1)$$

where F_{eq} is the equivalent radial force, C_r is the basic dynamic load rating, and d is the bearing type dependent exponent. Expression (1) is the core of the life computation procedure of the majority of the modern standards for analysis of bearings endurance, e.g., ISO 281 [3], ANSI/ABMA 11:2014 [4], and GOST 18855-13 [5]. With the aid of modification prefactors accounting for load, speed, oil viscosity, material fatigue limit, and content of contamination particles in the oil, this formula is still able to cover relatively large number of practical applications. However, the influence of the following factors remains unaccounted for:

- (1) bearing clearance,
- (2) flexibility of the bearing rings, housing, and shaft,
- (3) rings out-of-roundness,
- (4) inertia forces, acting on the rolling elements,
- (5) rolling elements profile, and
- (6) rings misalignment.

These factors can have a significant effect on maximum values of contact stresses and their distribution along each individual rolling element which in turn leads to redistribution of the resulting forces acting over the rollers.

Harris and Kotzalas [6] and Oswald et al. [7] have shown that slightly negative clearance increases bearing endurance as more rollers turn out to be in contact thus reducing the maximum radial force acting on the most heavily loaded one.

Considering bearing rings, deformations are particularly important for modern jet engines whose shafts are commonly hollow and the housing and the outer ring thicknesses may be of comparable magnitudes. Compliance of such bearing supports should not be omitted in analysis. Jones and Harris [8], studying planetary gear bearings (which are usually mounted in thin-walled housings), observed that excessive flexibility of the rings may reduce bearing life in default operating conditions, i.e., when the radial clearance is zero. However, they also demonstrated that as the internal clearance increases, rating life of bearings with rigid rings drops significantly faster than if the components were deformable. The authors found out that the peak rolling element loads occurred in close angular proximity to the points of load application. If clearance had been increased selectively at these points, maximum rolling element loads might have been reduced and fatigue life correspondingly could have increased. This gave rise to an idea of making the inner ring not perfectly circular, and this possibility was studied by Harris and Broschard [9] for various combinations of clearance and out-of-roundness intensity. It was shown that carefully adjusted ovalization of the ring can improve rating life by 40%. At the same time, such an alteration of the raceway shape imposes additional requirements on manufacturing accuracy, since if the geometry parameters of a non-circular ring are out of the permissible ranges, the bearing endurance can be seriously compromised.

It was demonstrated by Harris and Kotzalas [6] that another important factor, inertia acting on the rollers rotating about the

Contributed by the Tribology Division of ASME for publication in the JOURNAL OF TRIBOLOGY. Manuscript received February 16, 2021; final manuscript received May 10, 2021; published online June 10, 2021. Assoc. Editor: Wenzhong Wang.

shaft axis, increases the contact forces at the outer ring raceway. For small or slowly rotating bearings, this does not have significant effect, but for high speed ones, it may impact rating life quite significantly reducing it by an order of magnitude or even two.

The shape of the rolling element profile also seriously influences rating life. Such a modification of geometry of rolling elements is mandatory if bearing operational conditions imply the possibility of the rings misalignment. Oswald et al. [10] studied several most common roller profiles concluding that bearings with cylindrical rolling elements always have higher rating life. However, as also shown by Harris [11], non-profiled rollers exhibit significantly faster decrease of rating life once misalignment of the rings occurs.

To bring these factors into consideration for life assessments, the International Standard ISO 16281 [12] was developed. According to the approach proposed therein, the basic reference rating life is computed not from the external loads (radial and/or axial) but from contact forces arising between the rollers and the rings raceways. Of course, the distribution of these forces depends on the loads applied to the bearing, but this is only one of many other crucial factors which have been mentioned in the previous paragraphs. Moreover, for the case of radial roller bearings, ISO 16281 requires not only the resultant contact forces per roller to be determined but rather with their distributions along each rolling element. To obtain the results of even higher accuracy, one may additionally use information about pressures arising in the contact zones between rollers and raceways.

In the present work, a novel advanced approach for determining contact forces of a radial roller bearing with deformable rings and profiled rollers has been developed and combined with ISO 16281 for accurate assessment of rating life. The forces are computed taking into account the values of internal clearance, rotation speed of the shaft, external radial forces, rolling elements profile, and rings misalignment. This model is presented in Sec. 2. Its simplified version, which can be used for bearings with cylindrical rollers only, is also exposed. It serves as a tool for finding a good initial guess of the unknowns for the full featured bearing model. The numerical solution procedure is based on the Newton–Raphson method accompanied by the barrier functions technique initially designed for nonlinear optimization problems. The rings deformation is introduced as an arbitrary smooth function of internal forces which is detailed later in Sec. 3. The computational procedure of ISO 16281 for radial roller bearings is summarized in Sec. 4. To increase its accuracy, the profile of contact stresses between the roller and the rings raceways has to be determined. To this end, the method of Ahmadi et al. [13] for handling non-Hertzian contact of two elastic bodies has been adopted. Its main concepts are given in Sec. 5. Section 6 presents a numerical example of analysis of a radial roller bearing operating on various regimes with different clearances, external radial loads, and shaft rotation speeds. The influence of rings deformations, misalignment, and out-of-roundness on the rating life value has been studied. Section 7 summarizes the results of this work and identifies possible directions of further development of the proposed approach.

2 Bearing Model

When assessing rating life using ISO 16281, the key and, probably, the most important step is to find bearing equilibrium and determine internal contact forces. Most of the existing models of radial roller bearings which solve this problem omit structural deformations of rings. The approach of Harris and Kotzalas [6] handles radial roller bearings with rigid rings in the absence of misalignment. Tilting of the inner ring was added in the formulation of de Mul et al. [14] whereas structural flexibility was still missing. One of the first attempts to incorporate these deformations in static analysis of bearings was made by Filetti and Rumbarger [15] who treated the outer ring as a set of beam elements and used one-dimensional linear springs for the rollers in contact. This model proved to have good correlation with experimental data; however, a priori

knowledge about the attachment points of the outer ring significantly limits the approach applicability. Moreover, only one of the rings was considered deformable. The model of Cavallaro et al. [16], further extended by Leblanc et al. [17], accounts for deformations of both bearing rings. Distinctly from the previous formulations, the problem of determination of the rings deformations was formulated in terms of forces. The model also considered the centrifugal expansion of rings, the cage rotation, and the lubricant presence. However, only cylindrical rollers were handled by this approach and rings misalignment was also missing.

The approach presented in this section is aimed to eliminate the limitations of the aforementioned models and accounts for a larger set of factors when searching for the bearing equilibrium. A novel procedure based on the barrier functions method is specifically designed to ensure robustness of numerical solution of the governing equations.

2.1 Bearing Parameters. The geometry of the bearing cross section is depicted in Fig. 1. Subscripts “e” and “i” refer quantities related to the outer and inner rings, respectively. A special index $a = \{e, i\}$ which stands for either of the rings will denote a quantity or an expression that holds for both of them. Parameters R_s , R_h , and B_a are optional and required only for analysis with flexible rings. They are used to compute the a th ring cross-sectional area A_a , inertia moment I_a , and radius of the middle surface R_{ma} . In the current work, the cross sections of the rings are assumed to be rectangular, but they can be of any other shape—this does not limit the derivations presented below. Another important remark should be made regarding the term “ring.” Whenever it is further used within the text, the reader should understand not just the bearing ring itself, but the assembly of either the ring and the housing (for the outer) or the ring and the hollow shaft (for the inner).

The bearing has N rollers located at pitch radius R_p having angular distance $\theta = 2\pi/N$ between each other. A roller’s geometry is defined by its total length L , effective length L_{eff} , and maximum radius R_b . A rolling element may have a non-cylindrical profile, which is reproduced approximately using the slicing technique [14]. The roller in this case is discretized into K cylindrical slices (or laminae) as shown in Fig. 1. For the k th slice, one should define its radius b_k , width h_k , and distance s_k between its center and the roller central section.

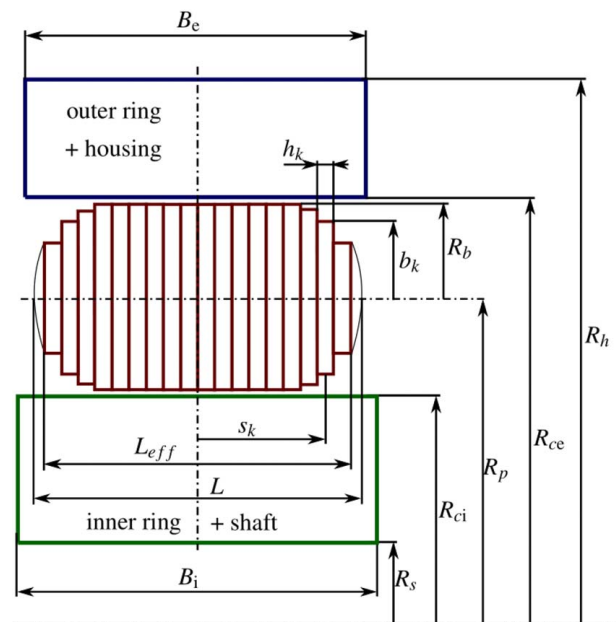


Fig. 1 Basic geometry parameters of the bearing and the slicing model of the roller

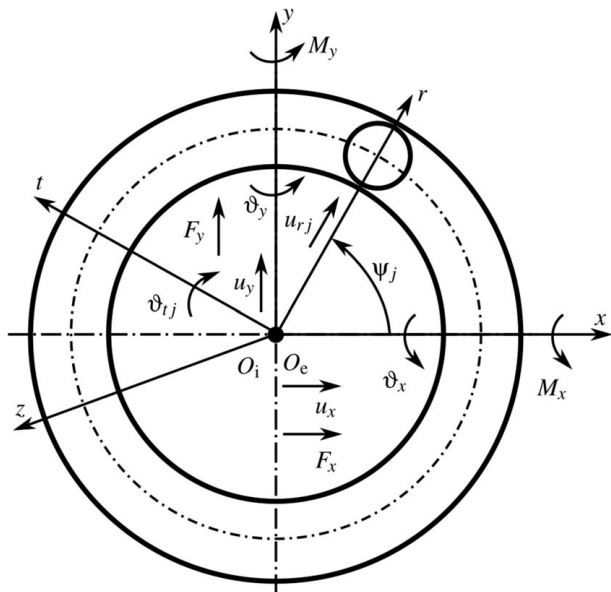


Fig. 2 Bearing coordinate system, inner ring loading, and degrees-of-freedom

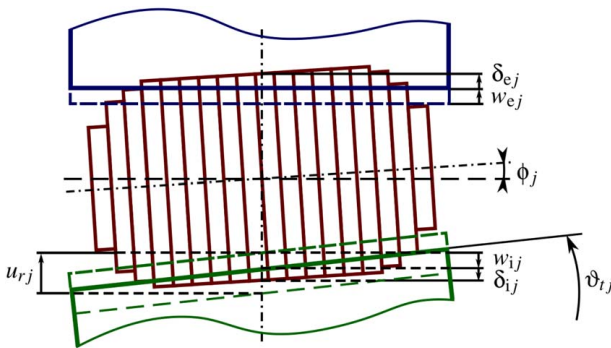


Fig. 3 Deformed configuration of the j th roller

2.2 Bearing Equilibrium. Consider a bearing as an element with two nodes O_i and O_e attached to the centers of the inner and outer rings, respectively, see Fig. 2. Node O_e is fixed and has the global Cartesian system x, y, z defined. Subject to external forces

$$\mathbf{F} = [F_x \ F_y \ M_x \ M_y]^T \quad (2)$$

the inner ring undergoes small displacements and rotations

$$\mathbf{y} = [u_x \ u_y \ \vartheta_x \ \vartheta_y]^T \quad (3)$$

with respect to node O_e . The model is not able to carry axial loading, so the component u_z is omitted.

Radial displacement u_{rj} and angular rotation ϑ_{ij} of the inner ring in the local coordinate system of the j th rolling element with angular position $\psi_j = (j-1)\theta$ can be determined as

$$\mathbf{y}_j = [u_{rj} \ \vartheta_{ij}]^T = \mathbf{S}_j \mathbf{y} \quad (4)$$

where

$$\mathbf{S}_j = \begin{bmatrix} \cos \psi_j & \sin \psi_j & 0 & 0 \\ 0 & 0 & -\sin \psi_j & \cos \psi_j \end{bmatrix} \quad (5)$$

Radial force Q_{ij} and moment T_{ij} arise between the ring raceway and the roller. The equilibrium equation of the entire bearing can then be written as

$$\mathbf{F} + \sum_{j=1}^N \mathbf{S}_j^T \mathbf{F}_j = \mathbf{0} \quad (6)$$

where the local roller's force vector has been introduced

$$\mathbf{F}_j = [Q_{ij} \ T_{ij}]^T \quad (7)$$

2.3 Roller Equilibrium. For the bearing roller compressed between the two rings, as depicted in Fig. 3, the following geometric relation holds:

$$g_{oj} + \delta_{ij} + \delta_{ej} + w_{ij} + w_{ej} - u_{rj} - u_{\theta j} = 0 \quad (8)$$

with $g_{oj} = g_o/2$, where g_o is the radial bearing clearance at a given regime; δ_{ij} and δ_{ej} are contact interferences of the rolling element into the raceways of the inner and outer rings, respectively; and w_{ij} and w_{ej} are radial deflections of the rings mid-surfaces. The latter quantities are presently not detailed and can be described by any continuous and one time differentiable function of radial forces

$$w_{aj} = w_{aj}(Q_{aj}), \quad n = 1, N \quad (9)$$

It is quite easy to introduce the predefined rings out-of-roundness [9] into Eq. (8) making g_{oj} dependent on the angular position with the aid of function $\chi(\varphi)$

$$g_{oj} = \frac{g_o}{2} + \chi(\varphi_j) \quad (10)$$

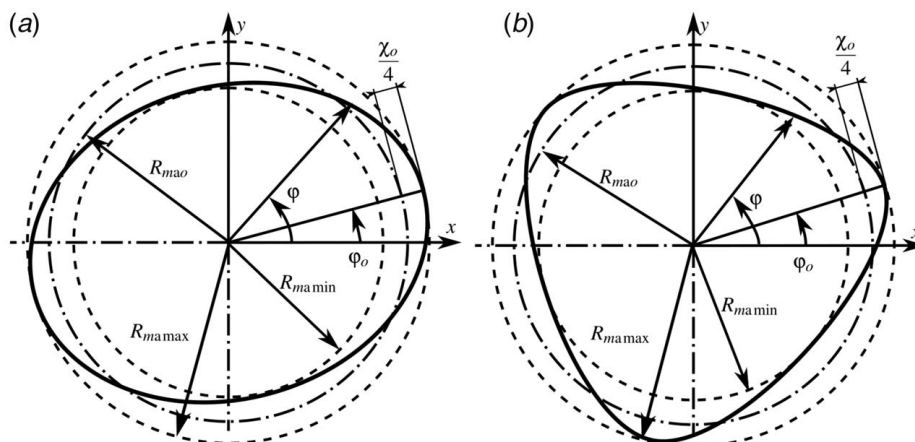


Fig. 4 Out-of-roundness of a bearing ring: (a) two lobes and (b) three lobes

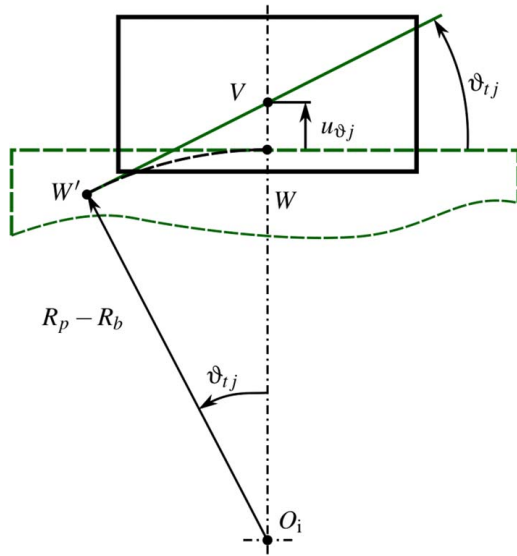


Fig. 5 Additional compression of the roller's center section due to the inner ring tilt

Normally, the geometry modification is introduced on a raceway of only one of the rings. Figure 4 shows two- and three-lobes out-of-roundness options which can be described by

$$\chi(\varphi) = \frac{\chi_o}{2} \cos \alpha(\varphi + \varphi_o) \quad (11)$$

where α is the number of lobes and

$$\chi_o = 2(R_{ma \max} - R_{ma \min}) \quad (12)$$

is the out-of-roundness magnitude.

Kinematic relation (8) also contains a small additional component $u_{\vartheta_{ij}}$ appearing due to the vertical deflection of the reference point used for the evaluation of compression of the central slice of the j th rolling element. Figure 5 shows how, when rotated at an angle ϑ_{ij} , the inner ring's point W moves to position W' and the central section of the roller is additionally compressed by

$$u_{\vartheta_{ij}} = O_i V - O_i W = (R_p - R_b) \left(\frac{1}{\cos \vartheta_{ij}} - 1 \right) \quad (13)$$

To perform computations accounting for the rings misalignment, the rolling element (even cylindrical) has to be divided into small laminae as shown in Fig. 1. The contact force q_{ajk} acting onto the k th slice of the j th roller from the contact surface of the a th ring can then be treated as Hertzian and thus described by the following expression [18,19]:

$$q_{ajk} = C_a h_k \delta_{ajk}^n \quad \text{with} \quad n = \frac{10}{9} \quad (14)$$

The compression of the k th slice is computed as

$$\delta_{ajk} = \delta_{aj} - R_b + b_k + \phi_{aj} s_k \quad (15)$$

where the misalignment angles of the roller with respect to each of the rings are given by

$$\phi_{ij} = \vartheta_{ij} - \phi_j \quad (16a)$$

$$\phi_{ej} = \phi_j \quad (16b)$$

Contact stiffness coefficient C_a depends on the materials properties. If rollers and rings are manufactured of the same material with

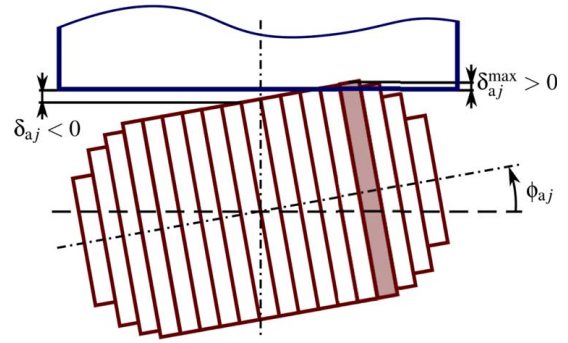


Fig. 6 Contact detection for the j th roller

Young's modulus E and Poisson's ratio ν , it is possible to write [19]

$$C_a = \frac{\pi E L_{\text{eff}}}{(1 - \nu^2)(7.358 L_{\text{eff}})^n} \quad (17)$$

The resultant force acting from the j th roller onto the a th raceway can then be computed as

$$Q_{aj} = \sum_{k=1}^K q_{ajk} \quad (18)$$

If misalignment angle $\vartheta_{ij} \neq 0$, the forces distribution along the roller j is not symmetric and generates moment

$$T_{aj} = \sum_{k=1}^K q_{ajk} s_{jk} \quad (19)$$

From Eq. (19), it is apparent why even a cylindrical roller has to be divided into at least two slices, otherwise $T_{aj} \equiv 0$. The roller equilibrium is therefore described by

$$\begin{cases} Q_{ej} = Q_{ij} + F_c & \text{with} \quad F_c = m \omega_r^2 R_p \\ T_{ej} = T_{ij} \end{cases} \quad (20a)$$

$$T_{ej} = T_{ij} \quad (20b)$$

where m is the roller mass and ω_r is its rotation speed about the central axis of the bearing.

2.4 Solution of the System of Nonlinear Equations. Expressions (6), (8), and (20) render the system of nonlinear equations with $3N+4$ unknowns: $u_x, u_y, \vartheta_x, \vartheta_y, \delta_{ij}, \delta_{ej}, \phi_j$, which can be merged into a single state vector

$$\mathbf{d} = [\delta_{ij} \quad \delta_{ej} \quad \phi_j \quad u_x \quad u_y \quad \vartheta_x \quad \vartheta_y]^T \quad (21)$$

The Newton–Raphson method can be applied to solve the system. To ensure the convergence of the iterative process, it is essential to fulfill the following $2N$ constraints naturally arising from the physics of the problem:

$$Q_{ij} \geq 0 \quad \text{and} \quad Q_{ej} \geq 0 \quad (22)$$

Recalling Eqs. (14) and (18), constraints (22) can be replaced with

$$\delta_{ij}^{\max} = \max_{k=1,K} \delta_{ijk} \geq 0 \quad (23a)$$

$$\delta_{ej}^{\max} = \max_{k=1,K} \delta_{ejk} \geq 0 \quad (23b)$$

Note that requiring $\delta_{aj} \geq 0$ is incorrect for meeting Eq. (22) since even if $\delta_{aj} < 0$ one may obtain $Q_{aj} \geq 0$ due to the presence of the rings misalignment angle, see Fig. 6. For additional stabilization of the iterative procedure, we also require that

$$u_x \text{ sign } F_x \geq 0 \quad (24a)$$

$$u_y \text{ sign } F_y \geq 0 \quad (24b)$$

$$\vartheta_x \text{ sign } M_x \geq 0 \quad (24c)$$

$$\vartheta_y \text{ sign } M_y \geq 0 \quad (24d)$$

To incorporate restrictions (24) into the solution algorithm, the method of logarithmic barrier functions is applied. This is a common tool [20] for handling a nonlinear optimization problem with J inequality constraints

$$\begin{aligned} \min \quad & \mathcal{F}(\mathbf{x}) \\ \text{subject to} \quad & \mathcal{H}_j(\mathbf{x}) \geq \mathcal{B}_j \quad \text{for } j = 1, \dots, J \end{aligned} \quad (25)$$

which, assuming $\mathcal{F}(\mathbf{x})$ and $\mathcal{H}_j(\mathbf{x})$ are all convex and twice differentiable functions, is equivalent to solving the following:

$$\min \quad \mathcal{G}(\mathbf{x}) = \mathcal{F}(\mathbf{x}) - \mu \sum_{j=1}^J \ln(-\mathcal{H}_j(\mathbf{x})) \quad (26)$$

As barrier height $\mu \rightarrow 0$, the closer $\mathcal{G}(\mathbf{x})$ gets to the original function $\mathcal{F}(\mathbf{x})$. Since the energy functional never appeared in the explicit form in the derivations above, the constraints (23) are directly incorporated into Eqs. (8) and (6) using the derivatives of the logarithmic barrier function as:

$$g_{oj} + \delta_{ij} + \delta_{ej} + w_{ij} + w_{ej} - u_{rj} - u_{\vartheta j} - \frac{\mu_\delta}{\delta_{ij}} - \frac{\mu_\delta}{\delta_{ej}} = 0 \quad (27)$$

and

$$\mathbf{F} + \sum_{j=1}^N \mathbf{S}_j^T \mathbf{F}_j - \mu_F \mathbf{B} = \mathbf{0} \quad (28)$$

where

$$\mathbf{B} = \begin{bmatrix} \frac{\text{sign} F_x}{u_x} & \frac{\text{sign} F_y}{u_y} & \frac{\text{sign} M_x}{\vartheta_x} & \frac{\text{sign} M_y}{\vartheta_y} \end{bmatrix}^T \quad (29)$$

The barrier heights μ_δ and μ_F should be chosen of different orders of magnitude since Eq. (27) is written for displacements while Eq. (28) for forces. For this reason, in numerical simulations, one should choose $\mu_F \gg \mu_\delta$. It is convenient to define barriers to be dependent on parameter ε :

$$\mu_\delta = 2^{-\varepsilon} \quad (30a)$$

$$\mu_F = \beta \mu_\delta \quad (30b)$$

where β is the scaling factor. The barriers height is then being gradually reduced by incrementing ε from ε_0 to ε_{lim} .

To ensure robustness of the iterative scheme for solving the system emerged from (20), (27), and (28), the initial value \mathbf{d}_0 should be carefully chosen, and for a general case it may be not straightforward. To assist with this step, a simpler analysis that disregards possible rings misalignment and rolling elements profiling is initially performed. Expression (18) can be explicitly inverted and merged with Eq. (14) in this case leading to

$$\delta_{aj} = \frac{Q_{aj}^{1/n}}{C_a} \quad (31)$$

and the original system of equations is replaced then with a simpler one

$$g_{oj} + \frac{Q_{ij}^{1/n}}{C_i} + \frac{(Q_{ij} + F_c)^{1/n}}{C_e} + w_{ij} + w_{ej} - u_{rj} - \frac{\mu_F}{Q_{ij}} = 0 \quad (32a)$$

$$F_x + \sum_{j=1}^N Q_{ij} \cos \psi_j - \frac{\mu_F \text{sign} F_x}{u_x} = 0 \quad (32b)$$

$$F_y + \sum_{j=1}^N Q_{ij} \sin \psi_j - \frac{\mu_F \text{sign} F_y}{u_y} = 0 \quad (32c)$$

where only $N + 2$ unknowns are remaining (Q_{ij} , u_x , u_y). This set of equations is less sensitive to the choice of the initial values of the unknown quantities and the barriers heights. It is convenient to choose the following initial guess:

$$\begin{cases} Q_{ij} = \max(F_c, 0.05F_x, 0.05F_y) & (33a) \\ u_x = 0.05 \|g_o\| & (33b) \\ u_y = 0.05 \|g_o\| & (33c) \end{cases}$$

The flowchart of the entire numerical process of determining the internal contact bearing forces is summarized in Fig. 7. For completeness, the scheme also contains the final two steps in the algorithm of computing the bearing rating life: solution of the non-Hertzian problem and invocation of the procedure from ISO 16281 [12]. These are further detailed in Secs. 5 and 4, respectively.

3 Rings Deformation

Nothing has been said yet regarding functions (9)—the only significant requirement is their continuity. The procedure for computing w_a is detailed herein.

To perform static analysis of a bearing ring subject to a set of external forces, one has to impose kinematic boundary conditions to prevent rigid body motions. It may not be straightforward to identify external kinematic constraints in practical cases. To circumvent this difficulty, Cavallaro et al. [16] proposed to treat the deformed shape of the ath ring as superposition of N deformations arising from each of the radial forces Q_{an} applied individually.

A given deformed shape of the ring emerged from a pointwise radial force Q_{an} can be decomposed [16,17] into Fourier series as

$$w_{an}(\varphi) = Q_{an} \sum_{p=0}^{\infty} \lambda_p \cos(p\varphi) \quad (34)$$

where

$$\lambda_0 = \frac{1}{2\pi} \int_{-\pi}^{\pi} w(\varphi) d\varphi \quad \text{for } p = 0 \quad (35a)$$

$$\lambda_p = \frac{1}{\pi} \int_{-\pi}^{\pi} w(\varphi) \cos(p\varphi) d\varphi \quad \text{for } p > 0 \quad (35b)$$

are physically nothing but compliance coefficients. According to the superposition principle valid for small deformations, deflection of the ring's mid-surface resulting from N radial forces Q_{an} , each acting at an angle ψ_n , can be expressed as

$$w(\varphi) = \sum_{n=1}^N w_{an}(\varphi) = \sum_{n=1}^N Q_{an} \sum_{p=0}^{\infty} \lambda_p \cos(p(\varphi - \psi_n)) \quad (36)$$

Coefficients (35) can be computed analytically, recalling, for instance, the solution for the ring subject to a pointwise radial force, applied at an arbitrary point, and equilibrated by tractions distributed with cosine profile [21] as exposed in Fig. 8

$$w_{an}(\varphi) = -\frac{Q_{an} R_{ma}^3}{4\pi E_a I_a} \chi(\varphi) \quad (37)$$

where

$$\chi(\varphi) = (\varphi - \pi) \sin \varphi + \left(\pi\varphi - \frac{\varphi^2}{2} + \frac{3}{4} - \frac{\pi^2}{3} \right) \cos \varphi + 2 \quad (38)$$

Introducing $\lambda_p = (R_{ma}^3 / 4\pi E_a I_a) \eta_p$, one may write the first five coefficients of the Fourier series expansion for function $\chi(\varphi)$

$$\eta_0 = 0, \quad \eta_1 = 0, \quad \eta_2 = \frac{4}{9}, \quad \eta_3 = \frac{1}{16}, \quad \eta_4 = \frac{4}{225} \quad (39)$$

Solution (37) disregards the kinematic boundary conditions imposed to the ring by its support that, in real situations, inevitably

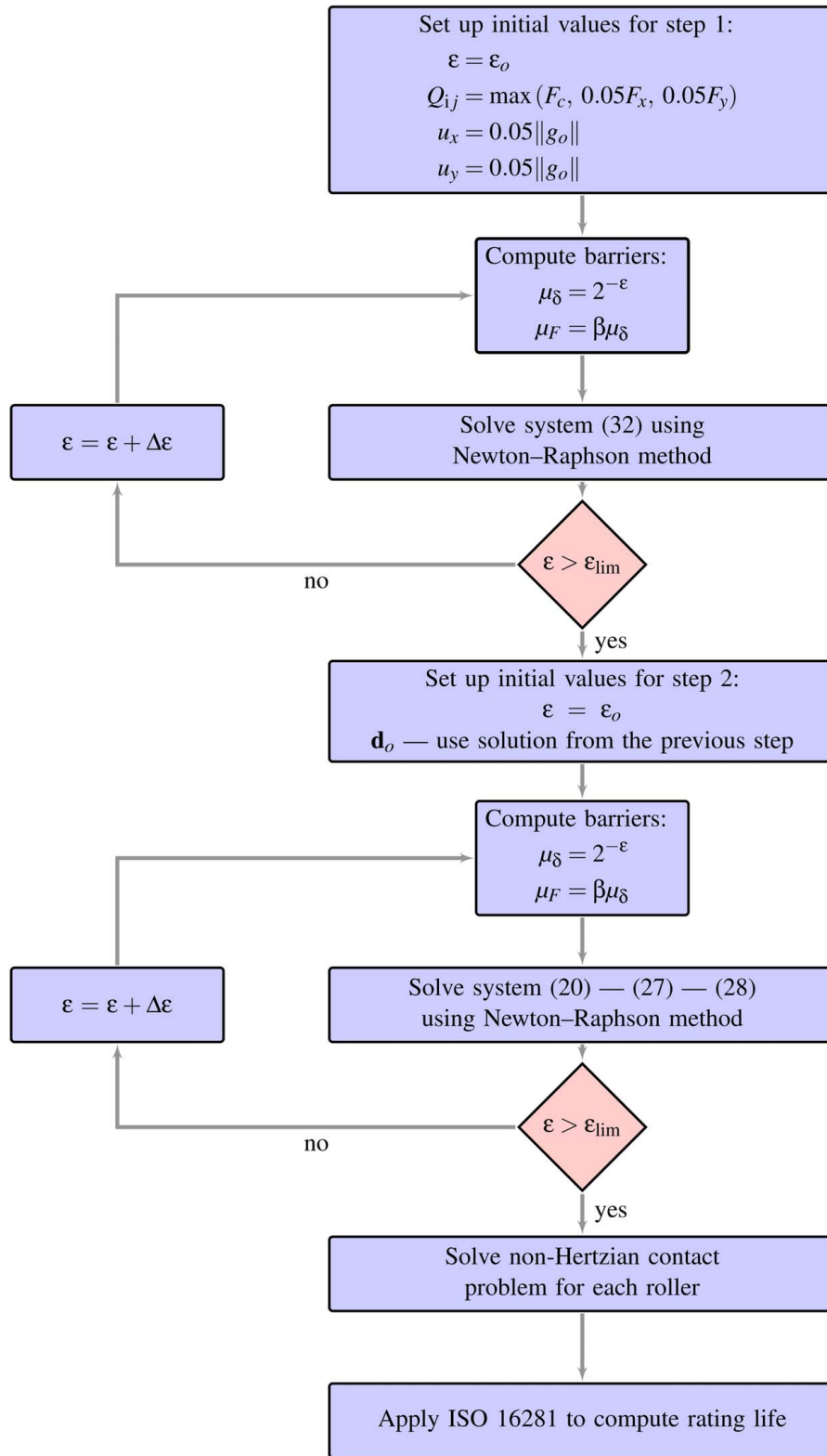


Fig. 7 Solution procedure for computing the bearing rating life

increases stiffness of the structure. Due to this fact, it is recommended to use a 3D model of the support-bearing assembly (of course, in the case of its availability) to compute λ_p more precisely. To this end, the corresponding three-dimensional spatial model is loaded by a unitary radial force at an arbitrary radial point as shown in Fig. 8. The obtained radial deflections are then used for numerical integration of expressions (35).

Representation of the deformed shape of the ring as Eq. (36) has some disadvantages. First of all, tensile deformations of the ring are omitted. Furthermore, if the profile of the acting radial forces tends to the shape of sin or cosine, i.e.,

$$Q(\psi) = Q_o + Q_b \cos \psi \quad (40)$$

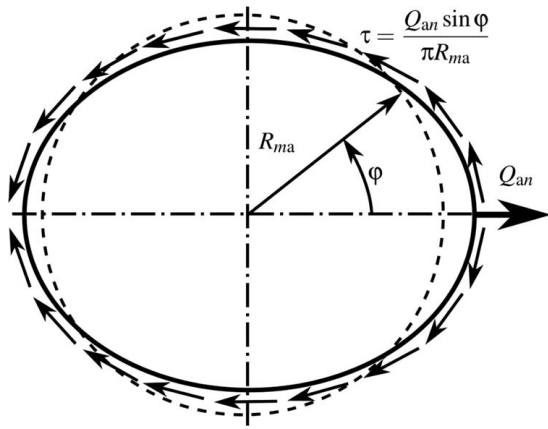


Fig. 8 A ring subject to a radial force and distributed tangential tractions

the resultant radial displacements $w(\varphi) \rightarrow 0$ as, due to orthogonality of individual members of expansion (34), the following terms entering (36) vanish:

$$\sum_{j=1}^N (Q_o + Q_b \cos \psi_j) \lambda_p \cos p(\psi_j - \varphi) = 0 \quad \forall p \neq N \quad (41)$$

Since the Fourier coefficients $\lambda_p \rightarrow 0$ as $p \rightarrow \infty$, for large values of N , term (41) tends to 0 even for $p=N$. It is apparent that precisely the same issue arises for the case of equal forces equidistantly distributed along the ring, i.e., when $Q_b=0$ and $Q_o \neq 0$ in (40).

This limitation is significant if either inertia forces act onto the ring or the bearing operates at a negative clearance. For such type of loading, the bending deformations are negligible while the tensile ones are of primary importance and can be treated separately using the analytical solution for the radial deflections of a ring subject to N identical equidistantly distributed forces [22]

$$w_a^{\text{tension}} = \frac{Q_a^{\min} R_{ma}}{E_a A_a \theta} \quad (42)$$

where

$$Q_a^{\min} = \min_{n=1, N} Q_{an} \quad (43)$$

Combining Eq. (42) with Eq. (36), one obtains the resultant expression for the deformations of a ring subject to a set of N radial forces:

$$w(\varphi) = \sum_{n=1}^N Q_{an} \sum_{p=0}^{\infty} \lambda_p \cos(p(\psi_j - \varphi)) + \frac{R_{ma} \min_{n=1, N} Q_{an}}{E_a A_a \theta} \quad (44)$$

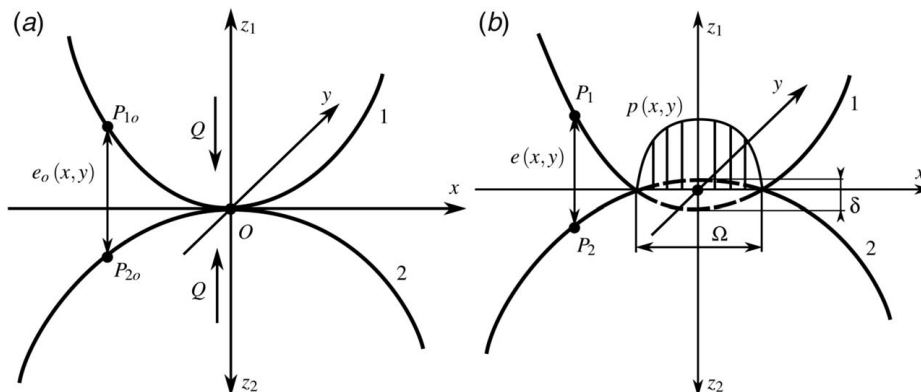


Fig. 9 Contact of two elastic bodies: (a) initial configuration and (b) deformed configuration

4 Bearing Life

The obtained distribution of the bearing internal forces can be effectively coupled with life computation methodology proposed in ISO 16281 [12]. Distinctly from ISO 281 [3], which relies solely on the values of the external radial and axial loads, the new standard introduces advanced calculation techniques which allow to account for bearing operating clearance, inertia effects, misalignment, roller profile, and rings flexibility.

As with ISO 281 [3], the basic dynamic radial load rating C_r is computed from the bearing geometry or provided by the manufacturer. This is then used to obtain the basic dynamic load ratings for each of the rings

$$Q_{ca} = \frac{1}{\lambda \nu \zeta_a N} \left(1 + \left(1.038 \left(\frac{1-\gamma}{1+\gamma} \right)^{143/108} \right)^{\xi_a} \right)^{2/9} \quad (45)$$

with $\lambda \nu = 0.83$, $\gamma = R_p/R_p$, $\zeta_i = 0.378$, $\zeta_c = 0.364$, $\xi_i = 9/2$, and $\xi_c = -9/2$. Quantities Q_{ca} are recomputed per individual lamina as

$$q_{cak} = \frac{Q_{ca}}{K^{7/9}} \quad (46)$$

ISO 16281 introduces specific functions describing stresses concentration over the j th roller evaluated for each slice

$$f_{ajk} = \frac{1}{q_{ajk}} \left(\left(\frac{p_{ajk}}{271} \right)^2 2R_b (1 \mp \gamma) \frac{L}{K} \right) \quad (47)$$

where sign “-” is chosen for $a=i$, and “+” for $a=e$. Here, p_{ajk} is the maximum value of the pressure acting in the contact zone between the j th roller and the a th ring raceway for the k th lamina. To compute p_{ajk} , the problem of non-Hertzian interaction has to be solved. Within the present work, the approach of Ahmadi et al. [13] has been adopted to tackle it. Its concepts and essential ideas are summarized in Sec. 5. Once the concentration factors f_{ajk} are available, the dynamic equivalent loads of the k th slice can be determined with

$$q_{dak} = \left(\frac{1}{N} \sum_{j=1}^N (f_{ajk} q_{ajk})^w \right)^{1/w} \quad (48)$$

Here, $w=4$ for the rotating ring and $w=4.5$ for the non-rotating one. Finally, the basic reference rating life can be computed as follows:

$$L_{10r} = \left(\sum_{k=1}^K \left(\left(\frac{q_{cik}}{q_{dik}} \right)^{-9/2} + \left(\frac{q_{cek}}{q_{dek}} \right)^{-9/2} \right) \right)^{-8/9} \quad (49)$$

5 Non-Hertzian Contact of Two Elastic Bodies

Let bodies 1 and 2 be initially in contact at point O , such that the distance between arbitrary points P_{1o} and P_{2o} , having common projection on the plane Oxy , is predefined via function $e_o(x, y)$ as depicted in Fig. 9(a). Subject to normal force Q , the bodies deform and interpenetration δ at point O arises. As the result of their elastic deformations, the contact area Ω is formed within which the pressure $p(x, y)$ acts, such that [13]

$$p(x, y) \geq 0 \quad (x, y) \in \Omega \quad (50a)$$

$$p(x, y) = 0 \quad (x, y) \notin \Omega \quad (50b)$$

According to the Boussinesq solution [23], with the contact pressure $p(x, y)$ applied, the displacement field of the surface of body 1 can be computed [24] as

$$u_{1z}(x, y) = \frac{1 - \nu_1}{2\pi G_1} \iint_{\Omega} \frac{p(x', y')}{\sqrt{(x-x')^2 + (y-y')^2}} dx' dy' \quad (51)$$

where ν_1 and G_1 are Poisson's ratio and shear modulus, respectively. The distance between the two points P_1 and P_2 in the deformed configuration is then given [25] by

$$e(x, y) = e_o(x, y) + u_{1z}(x, y) + u_{2z}(x, y) - \delta \quad (52)$$

see Fig. 9(b). Contact condition (50) can be rewritten with the aid of Eq. (52) as

$$e(x, y) = 0, \quad (x, y) \in \Omega \quad (53a)$$

$$e(x, y) \geq 0, \quad (x, y) \notin \Omega \quad (53b)$$

The distribution of the contact pressure has to equilibrate the external force Q [13,25], i.e.:

$$\iint_{\Omega} p(x', y') dx' dy' = Q \quad (54)$$

Integral equation (52), whose unknowns are $p(x, y)$, δ , and Ω , can be solved analytically only for the elliptic case and discrete schemes have to be applied for more complicated contacting objects. Ahmadi et al. [13] proposed the following simple but efficient numerical approach to cope with this problem. The computational domain consisting of finite number of cells has to be constructed such that its dimensions overestimate the area of the contact region Ω . Equations (52) and (54) are discretized replacing integration with summation over the computational domain considering pressure to be constant within each cell. The rendered system of linear equations is then solved providing the pressure values at each cell. Some of them will be negative, then the actual maximum stress will be overestimated. The cells having $p < 0$ are removed from computations and the procedure repeats until all the remaining cells of the computational domain have pressure $p \geq 0$ and equilibrium condition (54) is fulfilled. The detailed description of the entire procedure can be found in Ref. [13].

The Boussinesq solution (51) is obtained for the half-space situation [26] while in reality the contacting bodies have finite length and depth. This requires additional correction of the stress and displacement fields. To this end, the adjustments for the finite length and depth of the bodies proposed by Reusner [27] and later implemented by de Mul et al. [24] have been integrated in the present numerical scheme.

For rollers (either cylindrical or profiled), it is convenient to define function $e_o(x, y)$, that describes the initial geometry of the bodies, as follows:

$$e_o(x, y) = \left(\frac{1}{2\rho_{1x}} + \frac{1}{2\rho_{2x}} \right) x^2 + \left(\frac{1}{2\rho_{1y}} + \frac{1}{2\rho_{2y}} \right) y^2 + x \tan \phi_y \quad (55)$$

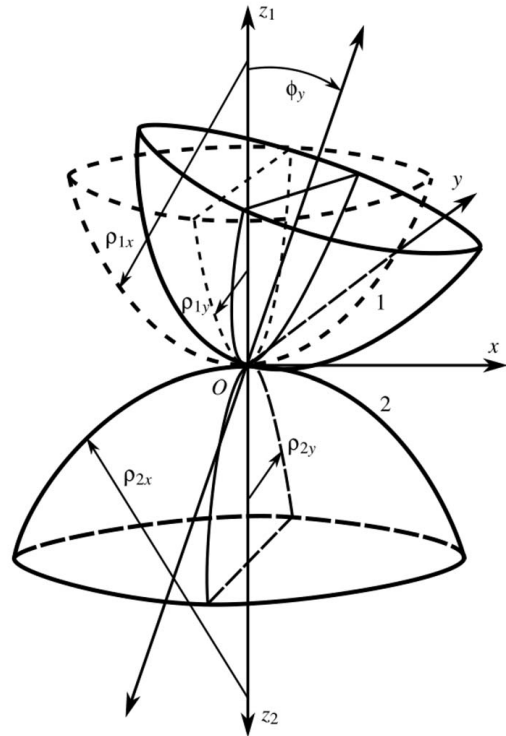


Fig. 10 Principle curvatures of the contact surfaces and influence of the misalignment on the geometry definition

where ρ_{1x} , ρ_{2x} , ρ_{1y} , and ρ_{2y} are the main curvature radii of the contact surfaces depicted in Fig. 10. For instance, if $\rho_{1y} = \rho_{2y} = \infty$ but ρ_{1x} and ρ_{2x} are constant, then one has classical Hertz problem of contact of two cylinders. Also note that if body 1 models a rolling element and body 2 a raceway surface, then $\rho_{2x} > 0$ for the inner ring and $\rho_{2x} < 0$ for the outer one. The last term in Eq. (55) accounts for misalignment between the roller and the ring.

6 Numerical Example

6.1 Bearing Data. Consider the radial roller bearing with pitch radius $R_p = 102.5$ mm having 32 rolling elements with maximum radius $R_b = 7.5$ mm, total length $L = 16$ mm, and effective length $L_{eff} = 14.5$ mm. The roller has crowned profile with $L_s = 6$ mm and $R_w = 1900$ mm as shown in Fig. 11. It is divided into 30

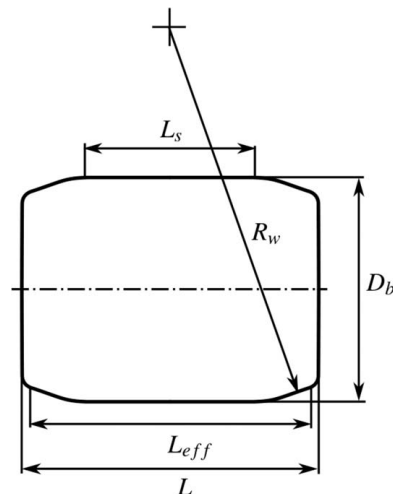


Fig. 11 A roller with crowned profile

Table 1 The bearing operating regimes

Regime	1	2	3
ω (rpm)	8500	9200	11,000
F_x (N)	5200	6300	7900
F_x/C_r	0.029	0.035	0.044
g_o (mm)	0.015	-0.007	-0.024

laminae along its effective length omitting the faceted edges. The inner ring is mounted on a hollow shaft with $R_i = 85$ mm and $B_i = 40$ mm and the outer ring is fitted in a thin-walled housing with $R_h = 240$ mm and $B_e = 40$ mm, see Fig. 1. All components of the bearing are manufactured of the same material whose elasticity modulus $E = 2 \cdot 10^5$ MPa, Poisson's ratio $\nu = 0.3$, and density $\rho = 7850$ kg/m³. The dynamic radial load rating $C_r = 178,000$ N, in accordance with ISO 281, is obtained from the bearing geometry.

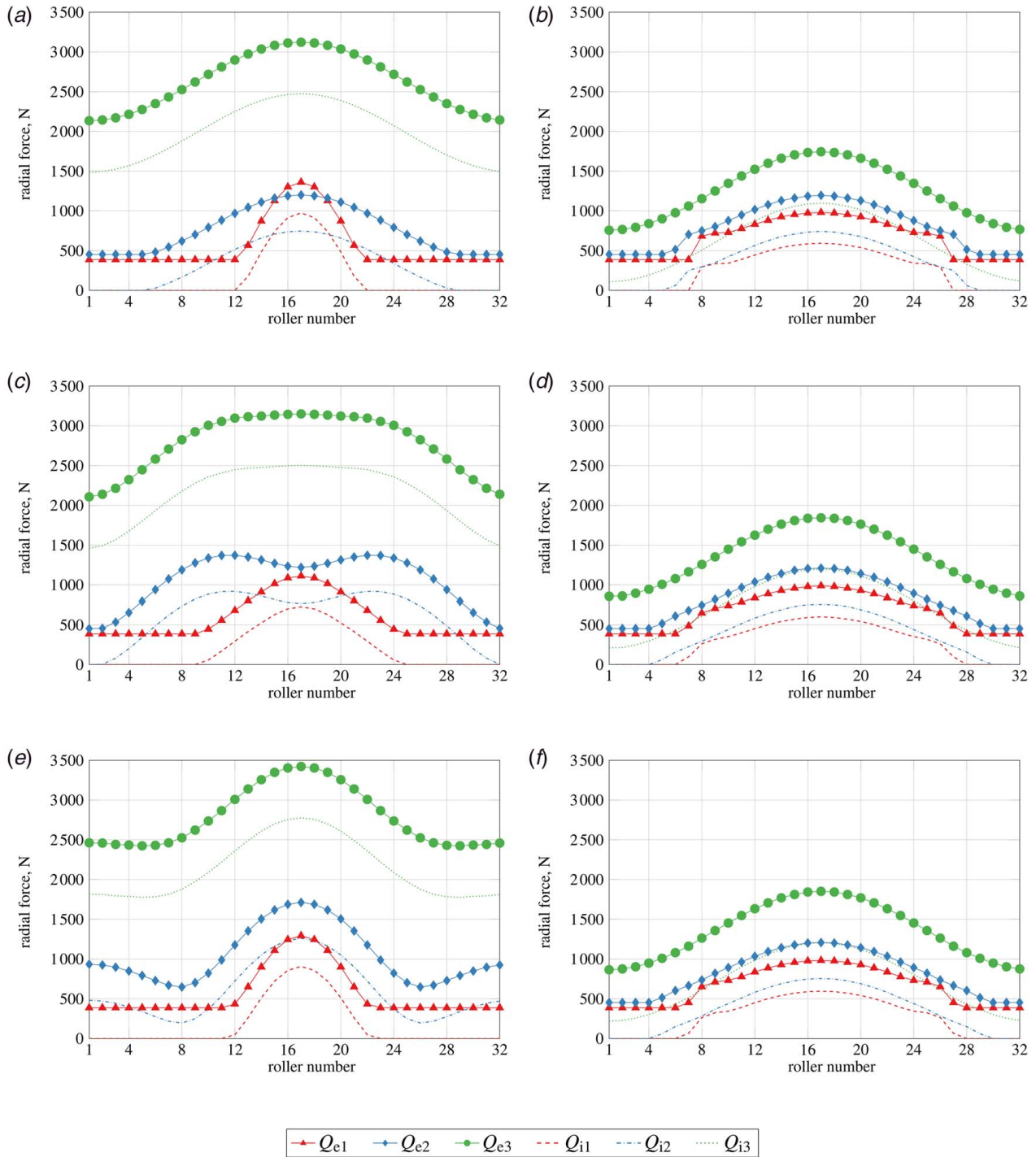


Fig. 12 Radial forces of the bearing for different loading conditions. (a) Rigid rings, no misalignment. (b) Deformable rings, no misalignment. (c) Rigid rings, misalignment $\vartheta_x = 6'$. (d) Deformable rings, misalignment $\vartheta_x = 6'$. (e) Rigid rings, misalignment $\vartheta_y = 6'$. (f) Deformable rings, misalignment $\vartheta_y = 6'$.

Table 2 The bearing rating life for different loading conditions (h)

Deformation	Misalignment	Regimes			Total
		1	2	3	
No	No	74,714	55,138	758	3609
Yes	No	107,324	49,241	10,211	30,734
No	$\vartheta_x = 6'$	66,527	7417	353	1566
Yes	$\vartheta_x = 6'$	46,622	22,395	4273	13,232
No	$\vartheta_y = 6'$	23,753	5764	341	1457
Yes	$\vartheta_y = 6'$	35,004	16,904	3552	10,586

The rolling elements are numbered such that the vector of the external radial load is directed from roller #1 towards roller #17.

A bearing with such a geometry can be commonly encountered in, for instance, a modern aircraft turbo engine. Usually the life of turbojet bearings is analyzed for a set of typical regimes with different radial and axial loads, rotation speeds, and temperatures of its components (which will define the change of the bearing clearance). For a bearing operating at a given regime s with known values of the radial force $F_{r,s}$ and the rotation speed of the inner ring ω_s , the rating life $L_{10r,s}$ is computed according with Eq. (49), in millions of revolutions. It is convenient then to obtain its equivalent in hours

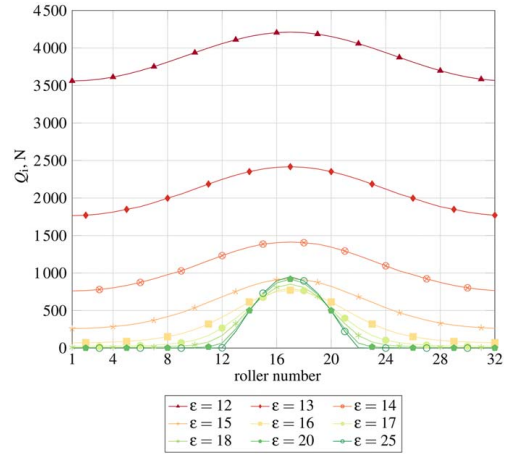


Fig. 13 Change of the distribution of the radial contact force Q_r for regime 1 along with the barrier height reduction

$$L_{hr,s} = \frac{10^6}{60\omega_s} L_{10r,s} \quad (56)$$

If the bearing operates at regime s for $\tau_s\%$ of the entire operation time, then the total bearing life $L_{hr,total}$ is calculated [28] as

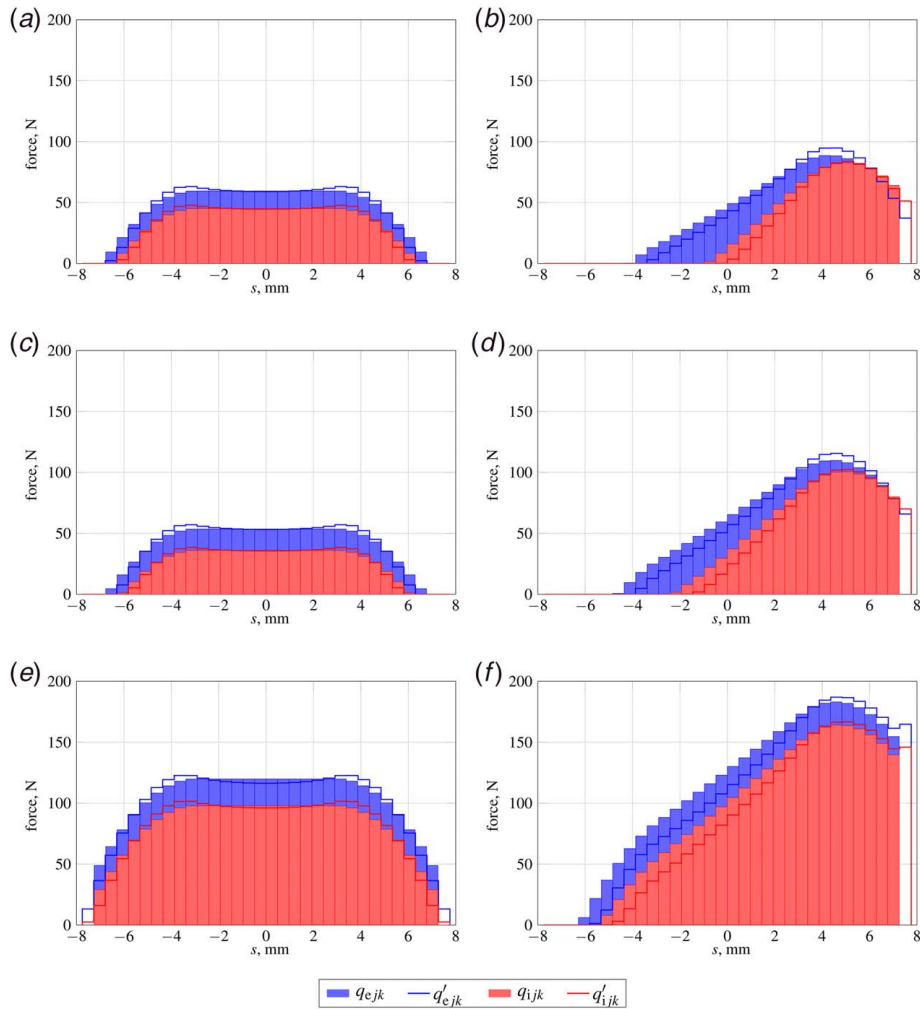


Fig. 14 Per slice forces along the contact line of roller $j = 17$, rigid rings case. (a) Regime 1, no misalignment. (b) Regime 1, $\vartheta_y = 6'$. (c) Regime 2, no misalignment. (d) Regime 2, $\vartheta_y = 6'$. (e) Regime 3, no misalignment. (f) Regime 3, $\vartheta_y = 6'$.

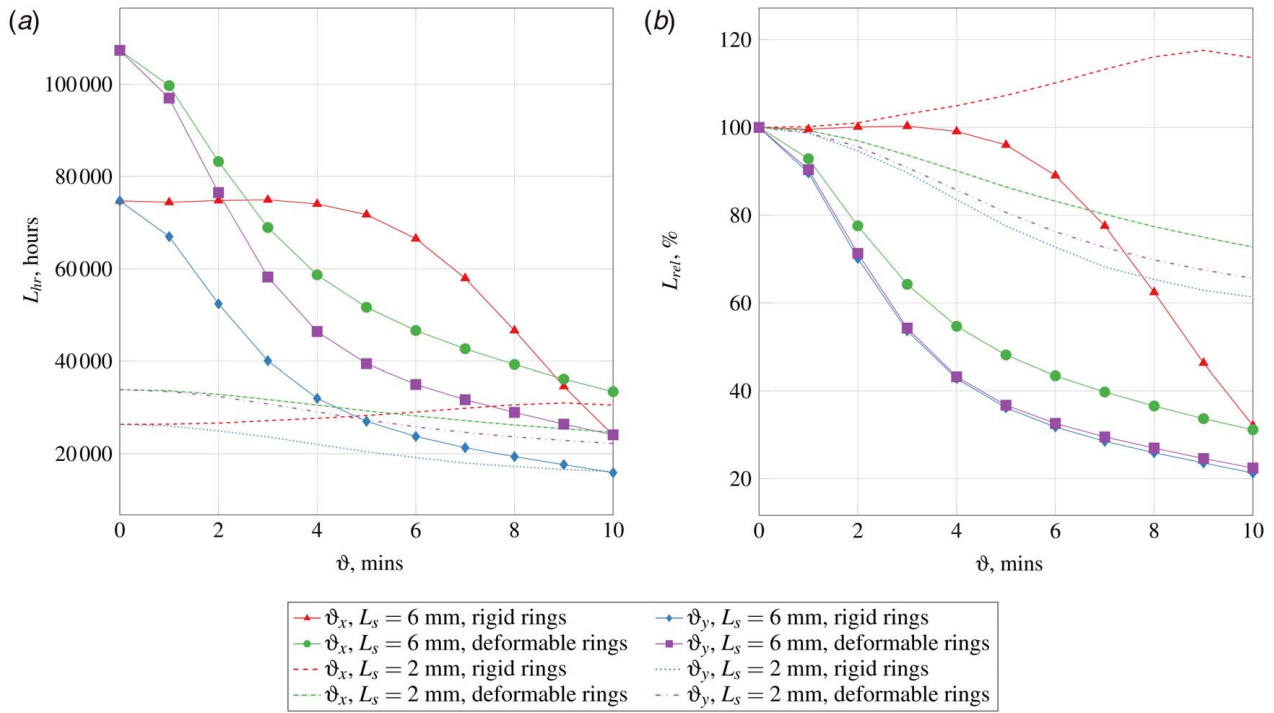


Fig. 15 Variation of the bearing rating life with respect to the misalignment angle: (a) variation of the rating life L_{hr} and (b) variation of the relative rating life L_{rel}

$$\frac{1}{L_{hr\ total}} = \sum_{s=1}^S \frac{\tau_s}{100L_{hr\ s}} \quad (57)$$

where S is the total number of regimes.

Three different regimes listed in Table 1 are used for the present analysis. The numbers correspond to the situations of lightly, heavily, and mildly loaded bearings. The clearances are intentionally chosen different to show the influence of this parameter on bearing endurance and to demonstrate the effect of bearing rings flexibility: different types of deformations prevail for positive (regime 1) and negative (regime 3) values of the internal clearance, and it is also interesting to see the behavior in the case of a nearly zero clearance (regime 2).

The bearing contact forces were computed according to the flow-chart plotted in Fig. 7, choosing the following barrier parameters: $\varepsilon_o = -5$, $\varepsilon_{lim} = 28$, $\Delta\varepsilon = 0.5$, and $\beta = 100$; residual relative norm with tolerance 10^{-6} was applied as a convergence criteria for the underlying Newton–Raphson scheme. For numerical solution of the non-Hertzian problem described in Sec. 5, a rectangular domain of 0.5×14.5 mm discretized with a mesh of 24×32 cells was used, see Ref. [13] for details.

6.2 Analysis Without Rings Misalignment. At first, let us demonstrate how rings flexibility influences the values of contact forces in the bearing and thus affects its life assessment. Figures 12(a) and 12(b) show the corresponding forces distributions and Table 2 contains the computed bearing life values. The deformations of the rings modify qualitatively profiles of the bearing radial contact forces for the first two regimes, but for the third regime no changes of this kind have been observed and still sinusoidal curve is obtained. This happens as for regimes 1 and 2 the dominant deformations are related to bending effects, while tensile strains prevail for the last one. Indeed, if we exclude the bending term from Eq. (44) and rerun simulation for regime 3, exactly the same distribution of the internal forces is obtained which is well explained by Eq. (41).

The bending effects arising in the rings for the first two regimes tend to bring more rolling elements into contact thus reducing the magnitude of the radial force acting on the most loaded one. In the majority of cases, like for regime 1, this increases bearing endurance, unless the distribution of internal radial forces is unusual (for instance, if out-of-roundness has been introduced on the contact surface of one of the rings). For the second regime, such rings deformations are obtained that no significant reduction of maximum Q_{aj} is observed but rather the redistribution of the radial forces results in a slight lowering of the bearing rating life.

It is also possible to detect in Fig. 12(a) that though the bearing clearance is negative, not all the rollers are in contact since penetrations of the rolling elements into the rings surfaces in the compressed part of the bearing compensate $g_o < 0$.

It is interesting to see the effect of the introduced barrier functions during computations. Figure 13 shows how the distribution of contact forces Q_i changes for regime 1 converging to the final result when ε is being gradually increased from 12 to 25 (this is equivalent to lowering μ_δ from $\approx 2 \cdot 10^{-4} \text{ mm}^2$ to $\approx 3 \cdot 10^{-8} \text{ mm}^2$).

6.3 Analysis With Rings Misalignment. The effect of rings misalignment is then studied. To demonstrate its influence on bearing endurance, the $6'$ tilt was alternately defined around axes x and y of the global coordinate system. In the case of rigid rings, both $\vartheta_x = 6'$ and $\vartheta_y = 6'$ introduce more rollers in contact comparing to the situation when misalignment was absent. The contact forces are redistributed not only over the rollers but also along their length increasing the gradient of q_{ajk} for those of them most suffering from the effect of misalignment: for $\vartheta_x = 6'$ these are the rolling elements with $j=9$ and $j=27$ and for $\vartheta_y = 6'$ with $j=1$ and $j=17$. The effect is reflected in Fig. 14 which shows quantities q_{ajk} for roller $j=17$ in the rigid rings situation in 2 cases: zero misalignment and when $\vartheta_y = 6'$. It is clear from Table 2 that when the inner ring tilts, the bearing rating life drops and for some cases may drop quite significantly.

One may notice that no significant difference can be seen between Figs. 12(b), 12(d), and 12(f) – the obtained force profiles are very close to each other. Again this is due to the effect of rings

flexibility which allows the bearing as a mechanical system to adapt to external loads so as to achieve an equilibrium position with a minimum of energy. However, even if the resultant forces look similar, the distribution of contact loads along each rollers becomes nonuniform due to rings misalignment (see Fig. 14) that will again inevitably reduce the bearing rating life.

Table 2 also shows that misalignment ϑ_x about the axis perpendicular to the vector of the external radial load is less dangerous for the bearing than ϑ_y , which is expected since in the latter case the highest gradients of q_{ajk} appear on the most

loaded rollers. This holds for both rigid and deformable rings situations.

6.4 Effect of Roller Profile. Let us track now the influence of misalignment on bearing life in more detail. As working conditions with positive clearance are more common in practice, regime 1 is chosen for the present study. A set of parametric computations is performed varying ϑ_x and ϑ_y in range $0' \dots 10'$ with increment $1'$. Variation of the rating life is summarized in Fig. 15(a). The plot

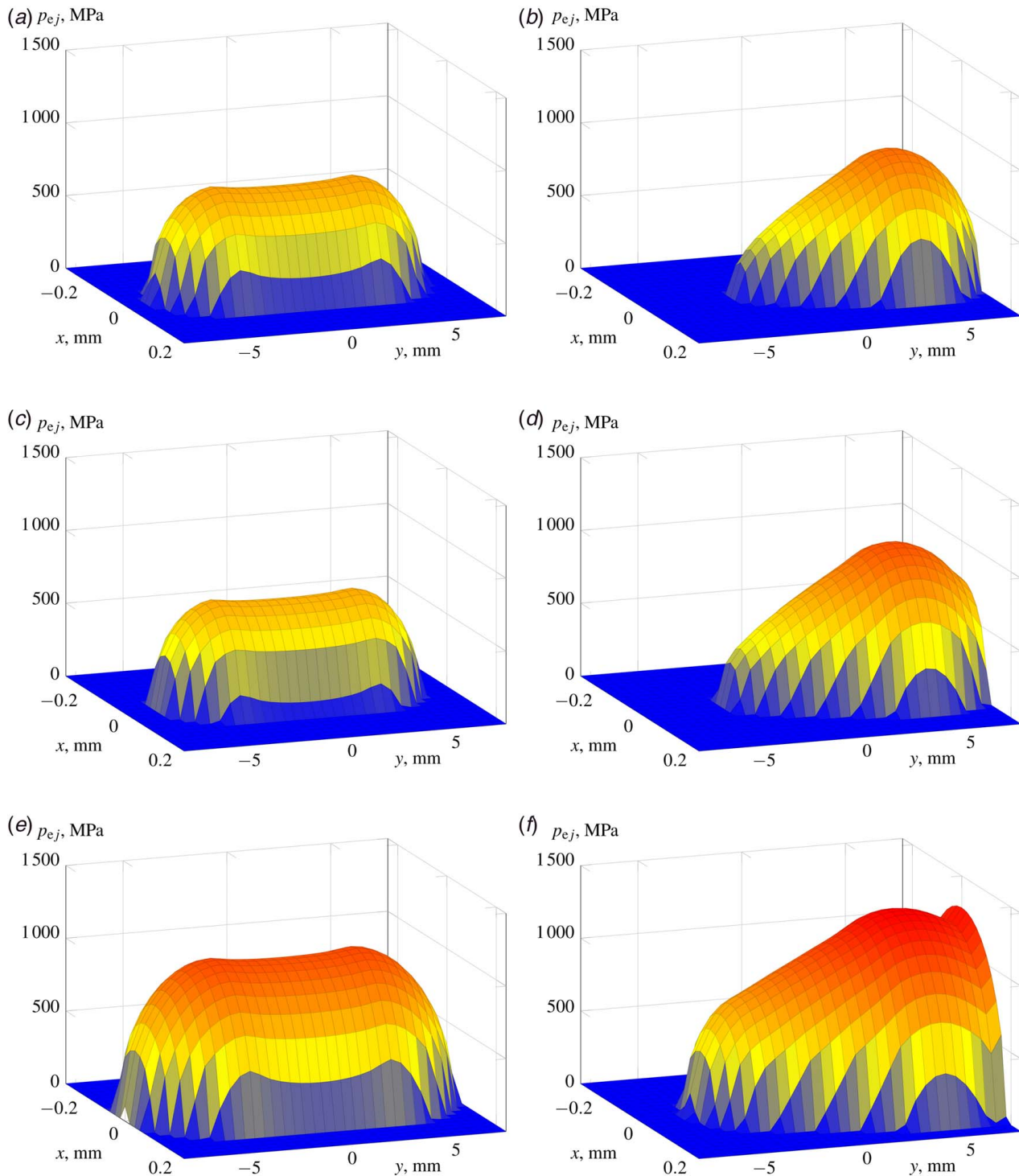


Fig. 16 Contact pressure distribution in the outer ring contact zone for roller $j = 17$, rigid rings case. (a) Regime 1, no misalignment. (b) Regime 1, $\vartheta_y = 6'$. (c) Regime 2, no misalignment. (d) Regime 2, $\vartheta_y = 6'$. (e) Regime 3, no misalignment. (f) Regime 3, $\vartheta_y = 6'$.

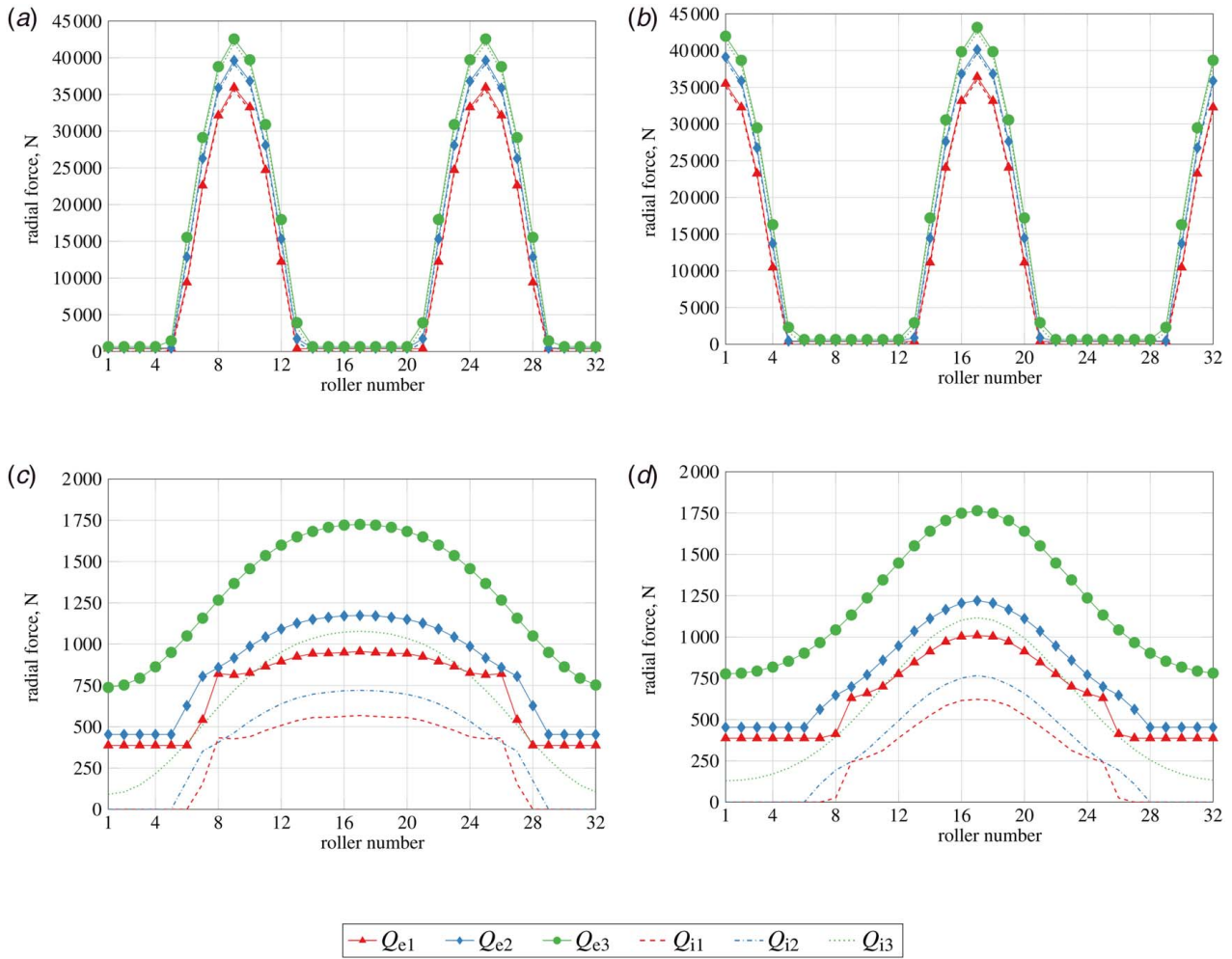


Fig. 17 Radial forces of the bearing when the outer ring out-of-roundness is introduced. (a) $\varphi_o = 0$, rigid rings. (b) $\varphi_o = \pi/2$, rigid rings. (c) $\varphi_o = 0$, flexible rings. (d) $\varphi_o = \pi/2$, flexible rings.

shows that thin deformable rings provide additional flexibility for optimal rearrangement of the internal contact forces that limits the drop of L_{hr} at large tilts—the result that has already been partially presented in Table 2. Figure 15(b) shows the evolution of the reference quantity

$$L_{rel} = \frac{L_{hr} \text{ with misalignment}}{L_{hr} \text{ without misalignment}} \quad (58)$$

to present this effect in a clearer comparative manner.

In Fig. 15, one may see that for the case of rigid rings with ϑ_x being varied, the bearing life remains almost unchanged until the ring angular deflection has reached $5'$. This happens, thanks to the rolling elements profiling. Eventually, the use of non-cylindrical rollers was proposed by engineers exactly for making bearings less sensitive to possible misalignments. The quantitative results agree well with the common recommendations [29] for radial roller bearings to operate at misalignment not exceeding $4'$.

It is interesting to see in Fig. 15 that if we reduce length of the straight part of the profiled roller to $L_s = 2$ mm, then the bearing becomes even less sensitive to misalignment. Moreover, with the increase of ϑ_x , the rating life grows (for the rigid rings model) or at least remains nearly constant (if rings are deformable). Though it may look surprising, but such a behavior is possible since for a small angular deflection ϑ_x the contact zone between certain rollers and a raceway enlarges that lowers maximum contact stresses thus improving endurance. However, looking at this seemingly better behavior of the more crowned bearing rollers with $L_s = 2$ mm, one should pay attention not only to the relative numbers but also to

the absolute ones: in the absence of misalignment, L_{hr} is three times lower than when $L_s = 6$ mm.

6.5 Contact Pressures. The replacement of the solution of non-Hertzian contact problem presented in Sec. 5 with an approximation introduced in Sec. 2.1 has some innate shortcomings. When dividing the contact body into laminae, it is assumed that shear effects between them can be neglected owing to the small magnitudes of the contact deformations that develop [30]. One should also keep in mind that the contact relation described by Eqs. (14) and (17) was originally derived for crowned rollers of finite length and then adopted for a single lamina. Given all this, it is reasonable to check plausibility of the slicing approach.

To this end, the distributions of contact stresses for roller $j = 17$ in the case of rigid rings were obtained using technique exposed in

Table 3 The bearing rating life when the outer ring out-of-roundness is introduced, flexible rings case (h)

χ_o	φ_o	Regimes			Total
		1	2	3	
0 mm	–	107,324	49,241	10,211	30,734
0.520 mm	0	91,016	42,170	9,120	26,966
0.520 mm	$\pi/2$	117,625	55,150	11,270	34,056

Sec. 5 and the corresponding surface plots for the outer ring (those for the inner one are very similar and thus omitted) are presented in Fig. 16. The obtained pressures p_{aj} can be postprocessed to compute the resultant force acting on the k th slice:

$$q'_{ajk} = \int_0^{x_c} \int_{s_k-h_k/2}^{s_k+h_k/2} p_{aj}(x, y) dx dy \quad (59)$$

where $x_c = 0.5$ mm is the nominal width of the computational domain when searching for the actual contact zone. The comparison of this quantity with q_{ajk} in Fig. 14 indicates that the simplification proposed by de Mul et al. [14] and adopted in the present model is accurate enough for practical applications. Good correlation between q_{ajk} and q'_{ajk} (in both situations when misalignment is absent and when $\vartheta_y = \delta'$) also validates Ahmadi's approach, see Sec. 5.

6.6 Effect of Out-of-Roundness. Let us show how the bearing life changes in the case of the two-lobes out-of-roundness of the outer ring with $\chi_o = 0.520$ mm. Two angular locations $\varphi_o = 0$ and $\varphi_o = \pi/2$ of the ellipse principal axis with respect to the external radial force vector are considered. Analysis with rigid rings for such geometry modifications is not relevant as it provides completely incorrect results: see internal forces distributions with enormous orders of magnitude plotted in Figs. 17(a) and 17(b). Distinctly from perfectly circular raceways, the geometries with out-of-roundness cannot be analyzed without incorporating rings flexibility into the model. The corresponding distributions of the radial contact forces for the three regimes from Table 1 in the case of the outer ring out-of-roundness with $\varphi_o = 0$ and $\varphi_o = \pi/2$ are shown in Figs. 17(c) and 17(d). Table 3 reveals that when the ring ovalization axis is perpendicular to the vector of the external radial force, the bearing rating life is improved by $\sim 10\%$ at each of the regimes, while the case $\varphi_o = 0$ lowers the bearing endurance approximately by the same percentage. The positive influence $\varphi_o = \pi/2$ was previously observed by Harris and Broschard [9] when studying the out-of-roundness of the bearing inner ring of the support of an idler gear in a planetary transmission.

7 Conclusions

An approach for radial roller bearing life analysis in complex loading conditions has been presented in the work. The formulation combines standard ISO 16281 for computation of the rating life with an advanced radial bearing model for determination of internal contact forces. This allows one to assess bearing endurance accounting not only for external radial loads applied to the inner ring but also for the (i) internal bearing clearance, (ii) rolling elements profile, (iii) inertia effects and rings, (iv) flexibility, (v) out-of-roundness, and (vi) misalignment. Conventional approaches based on ISO 281 can be hardly used for bearing life analysis if either of these factors becomes essential.

One of the key steps of the approach is computation of the distribution of contact forces over rolling elements of the bearing. To obtain them, a model of the radial roller bearing with structurally deformable and possibly misaligned rings has been proposed. Rings may exhibit bending and tensile deformations. The former are reproduced superimposing deformed shapes from each of the arising internal contact force acting individually. In the simplest case, the bending flexibility of a ring can be estimated from the existing analytical solution of the problem about the ring subject to a radial force equilibrated by distributed tractions. For more precise computations, the flexibility coefficients can be obtained by performing static analysis of the 3D model of the support-bearing assembly. Tensile strain is captured using the analytical solution for the ring subject to a large number of equidistantly distributed radial forces of the same magnitude. The presented benchmark test has shown sufficiency of this decomposition for practical applications.

The Newton–Raphson method, if applied directly to the resultant set of nonlinear equations, does not render immediately a stable numerical scheme since the constraints, which have to be fulfilled by the unknowns (the contact penetrations and forces cannot be negative), may become easily violated along the iterations. To stabilize the solution process and improve its convergence, the barrier functions technique, commonly used in nonlinear optimization problems, has been successfully adopted. According to this method, the inequality constraints are directly incorporated into the governing equations via logarithmic barriers. The obtained system is then solved multiple times constantly reducing the barriers heights that diminishes their influence on the contact forces distribution.

According to ISO 16281, to improve even further accuracy of rating life analysis, the distribution of contact stresses arising between a roller and a ring raceway and its possible concentration should be used in computations. A well-established numerical approach for solving non-Hertzian contact problems proposed by Ahmadi et al. [13] has been implemented in the present work to handle this step. This technique was also used to confirm the validity of the slicing approximation of the profiled roller geometry used in the bearing model for computation of contact forces along each rolling element.

The developed approach has been applied to a radial roller bearing of the geometry close to that what is presently used in industry for modern jet engines. The bearing rating life was computed for three regimes having different clearances, rotation speeds of the inner ring, and external radial loads. It was shown how the combination of these factors influences the distribution of contact forces. Thanks to the rings flexibility, a more optimal distribution of contact stresses can be achieved, that improves bearing endurance at a given regime. It was also demonstrated how misalignment of the rings and its orientation with respect to the vector of the external radial load may change the distribution of internal forces. It was exposed that structural deformations of the rings lower the negative effect of misalignment.

Effect of rolling elements profile on the rating life has been also studied. The proposed approach perfectly captures the well-known aspect of rollers profiling: more crowned rolling elements deliver lower bearing endurance in conditions when misalignment is absent but they are much less sensitive to its appearance in comparison to cylindrical ones (regardless of whether rings are considered rigid or flexible).

On the whole, the developed approach allows engineers to perform accurate life assessments of radial roller bearings operating in complex conditions. Currently, axial loading is omitted but it is tempting to see how the model performs for tapered roller bearings. The proposed approach also omits the presence of the cage, which in practice may influence the distribution of the internal bearing forces [31]. Given that its rotation speed will be involved in computations in this case, it becomes essential to account for lubrication. The rotation speed of the cage can no longer be computed from pure kinematics in the presence of lubricant and one has to consider the arising sliding of Hertzian contacts, which additionally leads to appearance of friction forces in the contact zones between the rollers and raceways [32]. Lubrication also alters the profile of the contact pressure between the rollers and the rings [33]. The authors intend to incorporate these factors into the model in the future. Extension of the model to ball bearings is another naturally coming possibility for its further development.

Conflict of Interest

There are no conflicts of interest.

Data Availability Statement

The authors attest that all data for this study are included in the paper.

Nomenclature

Scalars

b = radius of a slice, mm
 d = bearing type dependent exponent for computing the rating life
 e = distance between the contacting bodies, mm
 f = stress concentration function
 h = width of a slice, mm
 m = rolling element mass, kg
 n = exponent of the contact relation
 p = contact pressure, MPa
 q = contact force acting on a slice, N
 r = local radial axis of a roller
 s = coordinate of the central section of a slice, mm
 t = local tangential axis of a roller
 u = displacement of the inner ring, mm
 w = radial deflection of the ring mid-surface, mm
 A = ring cross-sectional area, mm²
 B = width of the cross section of an assembly of a ring and a housing/shaft, mm
 C = contact stiffness, N/mm⁽ⁿ⁺¹⁾
 E = Young's modulus, MPa
 F = external force applied to the inner ring, N
 G = shear modulus, MPa
 I = ring cross-sectional inertia moment, mm⁴
 J = number of constraints of an optimization problem
 K = number of slices
 L = total length of a roller, mm
 M = external moment applied to the inner ring, N mm
 N = number of roller
 O = center of the coordinate system
 P = point of an elastic body
 Q = radial contact force acting on a rolling element, N
 S = number of regimes
 T = moment resulting from contact forces acting on a rolling element, N mm
 V = point indicating additional compression due to the inner ring rotation
 W = point indicating center of the inner ring raceway at the roller cross section in the initial configuration
 e_o = initial distance between the contacting bodies, mm
 g_o = bearing clearance at the regime, mm
 q_c = basic dynamic load ratings of a slice, N
 q_d = dynamic equivalent load of a slice, N
 u_g = additional small compression due to the inner ring rotation, mm
 C_r = basic dynamic radial load rating, N
 F_c = inertia radial force acting on the bearing rollers, N
 F_{eq} = equivalent load, N
 L_{eff} = effective length of a roller, mm
 L_{hr} = basic reference rating life, h
 L_{rel} = relative reference rating life, %
 L_s = length of the straight part of a crowned roller, mm
 L_{10r} = basic reference rating life, in million revolutions
 Q_b = multiplier of the cosine term of the radial force expansion, N
 Q_c = basic dynamic load ratings of a ring, N
 Q_o = constant term of the radial force expansion, N
 R_b = maximum radius of a rolling element, mm
 R_c = radius of the contact surface of a ring, mm
 R_h = external radius of the housing, mm
 R_m = radius of the middle surface of an assembly of a ring and a housing/shaft, mm
 R_p = pitch radius, mm
 R_s = internal radius of the shaft, mm
 R_w = roller crown radius, mm
 W = point indicating center of the inner ring raceway at the roller cross section in the tilted configuration

x, y, z = global Cartesian coordinate system attached to the bearing outer ring
 α = number of lobes for defining the ring out-of-roundness
 β = barrier scaling factor, N/mm
 γ = bearing geometry parameter
 δ = elastic contact penetration, mm
 ε = parameter defining barrier height
 ζ = ring basic dynamic load rating factor
 ϑ = angular misalignment of the inner ring, rad
 θ = angular distance between the two neighboring rolling elements, rad
 λ = compliance coefficients, mm/N
 μ = height of a general logarithmic barrier function
 μ_F = barrier height for displacements and rotations of the inner ring, N mm
 μ_δ = barrier height for contact penetrations, mm²
 ν = Poisson's ratio
 ξ = ring basic dynamic load rating exponent
 ρ = radius of curvature of an elastic body, mm
 τ = percentage of the total operational time for a given regime, %
 φ = angular coordinate, rad
 ϕ = angular deflection of a roller, rad
 χ = ring out-of-roundness function, mm
 χ_o = out-of-roundness magnitude, mm
 ψ = angular position of a rolling element, rad
 ω = rotation speed of the inner ring, rpm or rad/s
 ω_r = rotation speed of a rolling element about the bearing axis, rpm or rad/s
 Ω = contact zone area, mm²
 \mathcal{B} = scalar value of the inequality constraint of an optimization problem
 \mathcal{F} = objective function of an optimization problem
 \mathcal{G} = augmented objective function of an optimization problem
 \mathcal{H} = inequality constraint function of an optimization problem

Vector and Matrices

\mathbf{d} = state vector
 \mathbf{d}_o = initial approximation of the state vector
 \mathbf{x} = state vector of an optimization problem
 \mathbf{y} = vector gathering inner ring displacements and rotations
 \mathbf{B} = matrix of barriers
 \mathbf{F} = external loads vector
 \mathbf{S} = transformation matrix

Subscripts

a = inner or outer ring
 e = outer ring
 i = inner ring
 j = rolling element index
 k = slice index
 l = contacting body index
 n = radial force index
 p = Fourier series term
 r, t = local coordinate system axes of a rolling element
 s = regime
 x, y, z = global coordinate system axes

References

- [1] Lundberg, G., and Palmgren, A., 1947, "Dynamic Capacity of Rolling Bearings," Acta Polytech. Mech. Eng. Ser., 1(3).
- [2] Lundberg, G., and Palmgren, A., 1949, "Dynamic Capacity of Rolling Bearings," ASME J. Appl. Mech., 16(2), pp. 165–172.
- [3] International Organization for Standardization, 2007, "ISO 281:2007. Rolling Bearings—Dynamic Load Ratings and Rating Life."
- [4] American Bearing Manufacturers Association, 2014, "ABMA 11:2014. Load Ratings and Fatigue Life for Roller Bearings."
- [5] Engineering Center EPK LLC, 2013, "GOST 18855-2013. Rolling Bearings. Dynamic Load Ratings and Rating Life."

- [6] Harris, T. A., and Kotzalas, M. N., 2006, *Rolling Bearing Analysis, 5th Edition: Advanced Concepts of Bearing Technology*, 5th ed., CRC Press, Boca Raton, FL.
- [7] Oswald, F. B., Zaretsky, E. V., and Poplawski, J. V., 2012, "Effect of Internal Clearance on Load Distribution and Life of Radially Loaded Ball and Roller Bearings," Technical Report, National Aeronautics and Space Administration.
- [8] Jones, A. B., and Harris, T. A., 1963, "Analysis of a Rolling-Element Idler Gear Bearing Having a Deformable Outer-Race Structure," *ASME J. Basic Eng.*, **85**(2), pp. 273–278.
- [9] Harris, T. A., and Broschard, J. L., 1964, "Analysis of an Improved Planetary Gear-Transmission Bearing," *ASME J. Basic Eng.*, **86**(3), pp. 457–461.
- [10] Oswald, F. B., Zaretsky, E. V., and Poplawski, J. V., 2015, "Effect of Roller Geometry on Roller Bearing Load-Life Relation," Technical Report, National Aeronautics and Space Administration.
- [11] Harris, T. A., 1969, "The Effect of Misalignment on the Fatigue Life of Cylindrical Roller Bearings Having Crowned Rolling Members," *ASME J. Lubr. Tech.*, **91**(2), pp. 294–300.
- [12] International Organization for Standardization, 2008, "ISO 16281:2008. Rolling Bearings—Methods for Calculating the Modified Reference Rating Life for Universally Loaded Bearings."
- [13] Ahmadi, N., Keer, L., and Mura, T., 1983, "Non-Hertzian Contact Stress Analysis for an Elastic Half Space-Normal and Sliding Contact," *Int. J. Solids Struct.*, **19**(4), pp. 357–373.
- [14] de Mul, J. M., Vree, J. M., and Maas, D. A., 1989, "Equilibrium and Associated Load Distribution in Ball and Roller Bearings Loaded in Five Degrees of Freedom While Neglecting Friction—Part II: Application to Roller Bearings and Experimental Verification," *ASME J. Tribol.*, **111**(1), pp. 149–154.
- [15] Filetti, E. G., and Rumbarger, J. H., 1970, "A General Method for Predicting the Influence of Structural Support Upon Rolling Element Bearing Performance," *ASME J. Lubr. Tech.*, **92**(1), pp. 121–127.
- [16] Cavallaro, G., Nelias, D., and Bon, F., 2005, "Analysis of High-Speed Intershaft Cylindrical Roller Bearing With Flexible Rings," *Tribol. Trans.*, **48**(2), pp. 154–164.
- [17] Leblanc, A., Nelias, D., and Defaye, C., 2009, "Nonlinear Dynamic Analysis of Cylindrical Roller Bearing With Flexible Rings," *J. Sound Vib.*, **325**(1–2), pp. 145–160.
- [18] Palmgren, A., 1959, *Ball and Roller Bearing Engineering*, SKF Industries, Philadelphia, PA.
- [19] Andréason, S., 1973, "Load Distribution in a Taper Roller Bearing Arrangement Considering Misalignment," *Tribology*, **6**(3), pp. 84–92.
- [20] Vanderbei, R., 2008, *Linear Programming: Foundations and Extensions*, 3rd ed., Springer, New York.
- [21] Liu, J. Y., and Chiu, Y. P., 1974, "Analysis of a Thin Elastic Ring Under Arbitrary Loading," *ASME J. Eng. Ind.*, **96**(3), pp. 870–876.
- [22] Budynas, R., Young, W., and Sadegh, A., 2012, *Roark's Formulas for Stress and Strain*, 8th ed., McGraw-Hill Education.
- [23] Kalker, J. J., and Van Randen, Y., 1972, "A Minimum Principle for Frictionless Elastic Contact With Application to Non-Hertzian Half-Space Contact Problems," *J. Eng. Math.*, **6**(2), pp. 193–206.
- [24] de Mul, J. M., Kalker, J. J., and Fredriksson, B., 1986, "The Contact Between Arbitrarily Curved Bodies of Finite Dimensions," *ASME J. Tribol.*, **108**(1), pp. 140–148.
- [25] Keer, L., Lee, J., and Mura, T., 1984, "A Contact Problem for the Elastic Quarter Space," *Int. J. Solids Struct.*, **20**(5), pp. 513–524.
- [26] Johnson, K. L., 1985, *Contact Mechanics*, Cambridge University Press, Cambridge.
- [27] Reusner, H., 1977, "Druckfl achenbelastung und ober fl achenverschiebung im w alzkontakt von rotationsk orpern," Ph.D. thesis, University of Karlsruhe, Karlsruhe.
- [28] Zaretsky, E. V., 2013, "Rolling Bearing Life Prediction, Theory, and Application," Technical Report, National Aeronautics and Space Administration.
- [29] FAG, 1999, "FAG Rolling Bearings. Fundamentals. Types. Designs."
- [30] Harris, T. A., 2001, *Rolling Bearing Analysis*, 4th ed., John Wiley & Sons, Hoboken, NJ.
- [31] Aramaki, H., Shoda, Y., Morishita, Y., and Sawamoto, T., 1988, "The Performance of Ball Bearings With Silicon Nitride Ceramic Balls in High Speed Spindles for Machine Tools," *ASME J. Tribol.*, **110**(4), pp. 693–698.
- [32] Aihara, S., 1987, "A New Running Torque Formula for Tapered Roller Bearings Under Axial Load," *ASME J. Tribol.*, **109**(3), pp. 471–477.
- [33] Dowson, D., Taylor, C.M., Childs, T.H.C., and Dalmaz, G., 1995, "Lubricants and Lubrication," Proceedings of the 21st Leeds-Lyon Symposium on Tribology, Institute of Tribology, University of Leeds, Leeds, UK, Sept. 6–9, 1994.